Effect of molten pool convection on pores and elements distribution in the process of laser cladding

Yan Shixing, Dong Shiyun, Xu Binshi, Wang Yujiang, Ren Weibin, Fang Jinxiang

(National Key Laboratory for Remanufacturing, Academy of Armored Forces Engineering, Beijing 100072, China)

Aastract: The molten pool convection has a great impact on elements and pores distribution during the laser cladding process. In this paper, the form of molten pool convection was investigate in terms of laser cladding NiCuFeBSi alloys on the substrate of gray cast iron and 45 steel. Results indicated that the distribution forms of pores and elements in the clad layer are uniform and dispersive due to the molten pool convection. Moreover, element distribution is also uniform without any slow transition from the bottom of clad layers to the top by means of electron probe microanalysis (EPMA). And according to the Gaussian distribution of energy in the YAG laser beams, it can be concluded that the driving force of convection is the surface tension gradient due to the non-uniform distribution of molten pool temperatures. Those of the laser thermal density, the molten pool temperature, the convective speed and the surface tension gradient are closely related with each other. It indicates that the temperature increases as the laser thermal density rising. The higher temperature is, the larger surface tension gradient will be as well as the convective speeds.

Key word: laser cladding; molten pool; convection; gray cast iron; surface tension gradient

CLC number: TH117 **Document code:** A **Article ID:** 1007-2276(2014)09-2832-08

激光熔覆过程中熔池对流运动对熔覆层气孔和元素分布的影响

闫世兴,董世运,徐滨士,王玉江,任维彬,方金祥

(装甲兵工程学院 装备再制造技术国防科技重点实验室,北京 100072)

摘 要: 激光熔覆时熔池对流运动对熔覆层成分和气孔缺陷分布具有较大影响。通过在灰铸铁和 45 钢两种基体上进行激光熔覆 NiCuFeBSi 系合金的工艺试验，对熔池的对流运动形式进行了机理分析与试验验证。结果表明,受熔池强对流运动影响,熔覆层气孔呈均匀弥散化分布趋势;且自熔覆层底部向顶部方向合金元素分布均匀,无缓慢过渡特征。根据 YAG 激光光斑能量的高斯分布特征,获得了熔池对流运动的驱动力是熔池温度分布不均形成的熔池表面张力梯度。而且熔池表面张力梯度与激光能量密度,熔池温度,熔体对流运动速度是彼此密切相关的。熔池对流运动机理分析表明,热流密度越高,温度越高,表面张力梯度越大,熔体对流运动速度越大。

关键词: 激光熔覆； 熔池； 对流运动； 灰铸铁； 表面张力梯度

收稿日期:2014-01-07； **修订日期:**2014-02-03

基金项目:“十二五”预研项目(51327040401);国家 973 计划(2011CB013403)

作者简介:闫世兴(1984-),男,博士生,主要从事激光熔覆再制造方面的研究。Email:ysxing1984neu@163.com

导师简介:徐滨士(1931-),男,教授,博士生导师,主要从事装备再制造理论研究。Email:syd422@sohu.com

0 Introduction

Laser cladding is quite a complex process accomplished with instantaneous non-equilibrium physical and metallurgical reactions generating, which induces a severe molten pool convection and a high speed non-equilibrium solidification of molten metals existing in the laser cladding process[1–3]. However, the molten pool convection is a key factor which determines the shapes, sizes, temperatures and elements distribution of cladding layers, which determine the geometric and mechanical properties finally. Currently, the molten pool convection has received lots of attentions [4–6] that focus on energy transfer analysis, momentum transfers and mass transfers. The numeric analysis and measure on-line for the temperature field and speed field of molten pool convection also have been performed[7–8]. However, there is still limited research on relations between the convection patterns and pores and elements distribution in cladding layers and more efforts are required.

In this study, to recover these relations, a new experimental method was absorbed that a laser beam was irradiated simultaneously on the two different substrates 45 steel and gray cast iron which had different carbon contents. According to the different redox reactions generated in those substrates, the effect of molten pool convection on pores and elements distribution was well represented.

Since pores always exist in the molten pool as laser cladding on the gray cast iron, it could be used to trace the pattern of molten pool convection with its locations. Similarly, element distribution measured by electron probe microanalysis (EPMA) was used for illustrating the effect of convections. Furthermore, the relations among molten pool temperature, the surface tension gradient and convection speed were also explored in this paper.

1 Materials and experimental procedures

Figure 1 shows a schematic view of laser cladding process. The substrates used in this experiment were HT250 and 45 steel. And the laser cladding powders was NiCuFeBSi alloy which had a great forming quality. Chemical compositions of these materials were listed in Tab.1. Compared with HT250 generating lots of pores in the molten pool, 45 steel would produce less pores because of its low carbon contents. Thus, the pattern of molten pool convection could be researched by tracing the location of pores in the layer.

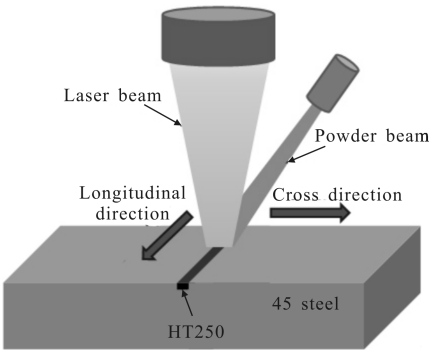

Fig.1 Scheme of laser cladding process along the cross and longitudinal directions

Tab.1 Components of the cladding powder and substrates

Element		C	S	P	Mn	Si	B	Cu	Fe	Ni
Content (wt%)	HT250	3.3–3.5	<0.05	<0.05	0.5–0.7	1.5–1.9	–	0.4–0.6	bal	–
	45 steel	0.42–0.5	<0.04	<0.04	0.5–0.8	0.17–0.37	–	–	bal	<0.3
	NiCuFeBSi	–	–	–	–	0.5~2	0.1–1	10–15	0.5–1	bal

A 100 mm×1 mm×4 mm (l*w*h) fillister was fabricated on the thick plate of 45 steel, then the same size banding sample was cut down from the HT250 and fixed into that fillister. A continuous wave YAG laser was used for laser cladding at conditions of laser power 1 000 W, powder feeding rate 5.76 g/min, scanning speed varied from 200 to 600 mm/min along the cross and longitudinal directions respectively. And

it presented that great formation quality of claddings had been obtained under those conditions [9]. The diameter of laser spot was 3.5 mm so that a single cladding layer could cover the top surface of fillister. Meanwhile, molten pool was shielded by pure argon.

The samples were cut to observe the microstructure and porosity distribution in the cross-section and longitudinal section of the cladding layer and then polished with a polishing machine. Finally, samples were etched by a 4% nital to allow a precise microstructural view. The distribution of C, Fe, Ni and Cu elements were measured by electron probe microanalysis (EPMA) in the layer.

2 Results and discussions

2.1 Character of pores distribution

Figure 2 shows the micrograph of longitudinal section in the cladding layer. It can be seen that no pores existing in the layer above the substrate of 45 steel, which indicates that the source of pores generation is due to the higher carbon contents (graphite) in HT250 than 45 steel. While graphite will

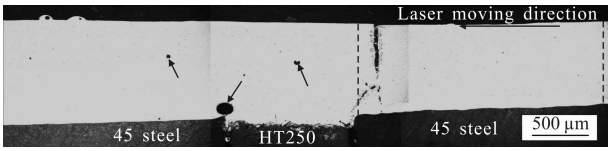

Fig.2 Longitudinal section patterns of cladding layers (with scanning speed 200 mm/min)

produce CO during laser cladding process cause the reaction of the oxygen and graphite. However, some pores are found in the latter forming layer which is above the substrate of HT250 and 45 steel. In contrary to the influence of pores self-buoyancy that will make pores floating vertically, the float trace of pores observed in the section of cladding has presented that pores floating path is not vertical but flexural. Therefore, there must be some factors interrupting the floating process of pores. It can be concluded that a severe convection should exist in the molten pool which makes the pores distributing to the latter forming layer which is above the substrate of 45 steel. Meanwhile, it is also noticed that substrate elements diluting into the molten pool can diffuse to a long distance.

Figure 3 shows the cross section patterns of NiCuFeBSi alloy layers with different scanning speeds. It can be seen that the pores distribute uniformly in the whole layer and break through the area of layers which is above the substrate of HT250. Therefore, it is known that main factors affecting pore distribution is the molten pool convection instead of the pores self-buoyancy. As laser scanning speed increased from 200 to 400 mm/min, pore sizes enhanced (Fig.3(b)). Moreover, some large sizes of pores exist at the bottom of cladding layers where are close to the interface between the cladding layer and HT250 because of the effect of rapid solidification of pools. Therefore, with increasing of laser scanning speed, the pore distance to bottom also declines as shown in Fig.3(a) and (b).

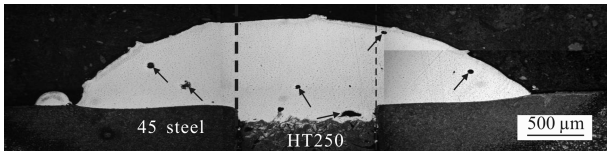

(a) A scanning speed of 200 mm/min

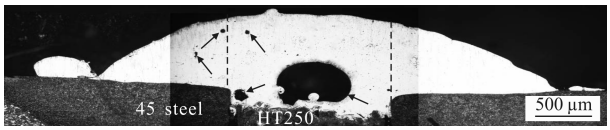

(b) A scanning speed of 400 mm/min

Fig.3 Cross section patterns of NiCuFeBSi alloy layers with different scanning speeds

Figure 4 shows the variation of pores character in the parallel section of NiCuFeBSi alloy layers at the different scanning speeds. A few small pores are shown in the layer with scanning speeds of 200 mm/min, while large pores are shown in the layer with speeds of 600 mm/min. Generally, pores size and distributing location is closely related to the temperature gradient of molten pool which decides the cooling rate of molten pool. With increasing of the scanning speed,

the temperature gradient raised, while the cooling rate of molten pool declined. Therefore, it can be concluded that the pores are trapped in the layer by rapid cooling of weld pool, and on the contrary at the lower cooling rate caused by the low scanning speed, pores can easily escape from the molten pool surface.

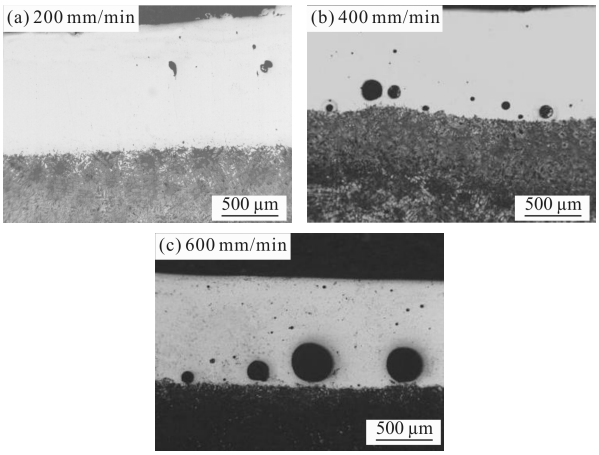

Fig.4 Pores characterization with different scanning speeds (laser power 1 000 W, powder feeding rate 5.76 g/min)

Compared to the patterns of pore distribution as HT250 fixed in the center of cladding layers, Figure 5 shows patterns of cross section as the HT250 arranged at the edge of cladding layer. Not unexpectedly, pores still distribute uniformly in the whole layer. Therefore, experimental results indicate that the severe molten pool convection affects pores distribution in the whole molten pool. In other words, such patterns of pores distribution are harmful for the properties of cladding layers, because so many pores distributing in the clad makes the clad structure loosely that will reduce the layers compactability as well as the tensile strength. It can be deduced that once a microcrack generates in the claddings then it will propagate rapidly along pores especially the large size of pores.

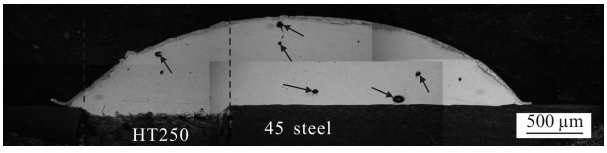

Fig.5 Patterns of cross section as the HT250 arranged at the edge of cladding layer (with scanning speed 200 mm/min)

Based on Fig.2 to Fig.5, it can be concluded that the pores are derived from redox reaction of gray cast iron substrate. While the main alloying elements in gray cast iron are carbon and silicon. The following redox reactions are possible during laser cladding process;

$$[Si]+2[O]=<SiO_2> \quad (1)$$

$$[C]+[O]=\{CO\} \quad (2)$$

$$<SiO_2>+2[C]=[Si]+2\{CO\} \quad (3)$$

The generating of {CO} pores were assumed to be due to the incomplete molten pool protection during laser cladding. Some oxygen than equilibrium content can be introduced to the melt from the atmosphere. By the oxidation of cast iron melt $<SiO_2>$ was generated in temperatures below 1 673 K and {CO} was formed in temperatures over 1 673 K[10]. Generally, gray cast iron is melted below 1 673 K and then heated up above 1 773 K just before tapping. Therefore, when cast iron is melted to over 1 673 K, $<SiO_2>$ suspended in the molten pool is reduced by [C] and then more {CO} gases are generated in the molten pool. Pores can be formed when this {CO} gas is captured in the molten pool.

2.2 Element distribution in the cladding layer

Figure 6 shows the elements distribution near the interface of cladding layers by line scanning of EPMA. Main elements of C, Fe, Ni and Cu were measured. It can be seen that C contents vary insignificantly at two sides of interface except the graphite location in the substrate. Similarly, the contents of Fe, Ni and Cu vary significantly at two sides of interface, especially in semi-molten zone of cladding layers. The content of Fe in the semi-molten zone is high then become uniform in a short distance to the interface as well as the elements of Ni and Cu. According to the distribution tendency, it can be seen that elements of Fe, C, Ni and Cu all distribute uniformly in the cladding layer, especially Fe and C which is mainly from the substrate. However, this result is reverse to the Fick′s diffusion law that elements content distributed into the molten attenuates gradually with the decrease of elements density due to

the reaction of substrate elements dilution. Therefore, it can be concluded that the elements distribution in the cladding layer are affected not only by the free dilution but also by the severe convection of molten pool which makes element distributing uniformly in a short time.

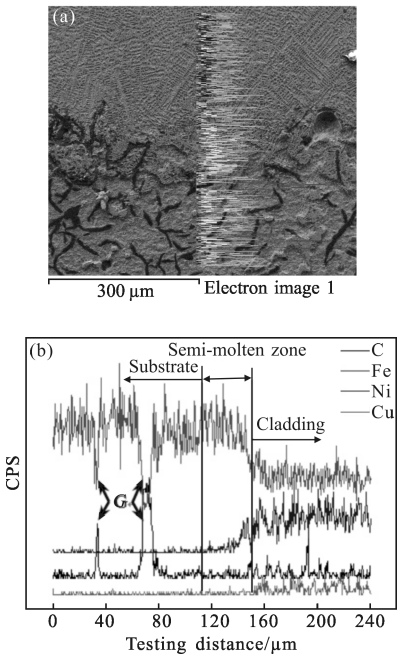

Fig.6 Element distribution near the interface of cladding layers (by line scanning of EPMA)

2.3 Molten pool convection

The experimental results have indicated that the convection of molten pool is the key factors affecting the pores and elements distribution. However, it depends on the surface tension gradient which resulted from the non-uniform distribution of molten temperatures. This surface tension gradient makes the melt metal flowing form a low tension part to a high one then molten pool convection formed. Therefore, it´s necessary to investigate the distribution of molten temperatures in order to characterize the pattern of molten pool convection. Moreover, the convection speed has been obtained based on the analysis of the molten pool temperature changes.

Since the energy distribution of YAG laser meets a Gaussian rule. Schematic view of energy distribution is shown in Fig.7. And the laser thermal density $q(r)$ in the laser spot has been given as Eq.(4) according to references[11]

$$q(r)=\frac{3Q}{\pi r_h^2}\exp\left(-\frac{3r^2}{r_h^2}\right) \tag{4}$$

Where r_h refers to the radius of laser spots focused on the substrate. According to Fig.7, the thermal density $q(r)$ is maximum to q_{max} when distance to the center $r=0$. Thus, substituting $r=0$ into the Eq.(4) the total thermo Q of laser irradiation into the molten pool can be obtained as follow:

$$Q=\frac{q_{max}\pi r_h^2}{3} \tag{5}$$

Where q_{max} refers to the maximum thermal density in the spots center. However, the laser cladding is a dynamic process. The thermal density distribution of molten pool is asymmetrical due to the Gaussian distribution patterns of laser energy. Experimental observation has presented that the shape of molten pool appears to be a double-half-ellipse who have both a short front semiaxis and a long back semiaxis[12]. Given that the thermal distribution along the deepness direction, the whole thermal distribution of molten pool can be considered as a double-half-ellipsoid which is shown in Fig.8.

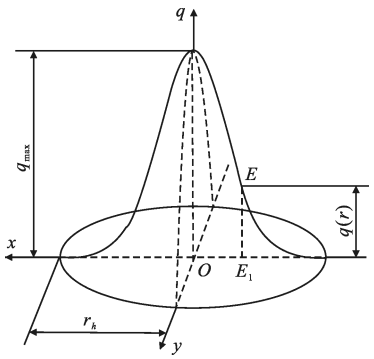

Fig.7 Gaussian distribution of energy in the laser beams

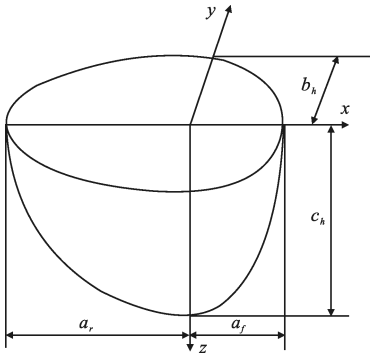

Fig.8 Schematic view of the double-half-ellipsoid distribution of thermo in the molten pool

In order to calculate the thermal density $q(r)$ in the double-half-ellipsoid, some assumptions are made;

The semiaxis of double-half-ellipsoid are respectively (a_r, b_h, c_h) and (a_f, b_h, c_h). The core coordinate is $(0,0,0)$, and the thermal density here is q_{max}. Then the thermal density in the double-half-ellipsoid can be written as:

$$q(x,y,z)=q_{max}\exp(-Ax^2-By^2-Cz^2) \quad (6)$$

Where A, B, C refer to the volume distribution coefficients of thermal density, respectively. The heat input of double-half-ellipsoid can be separated into two parts with proportions of f_r and f_f. where

$$f_r+f_f=1 \quad (7)$$

For instance of the left half-ellipsoid, the relation between heat input and thermal density can be given as follow:

$$f_r\cdot Q=2\int_0^{\infty}\int_0^{\infty}\int_0^{\infty} q(x,y,z)\mathrm{d}x\mathrm{d}y\mathrm{d}z=\frac{q_{max}\pi\sqrt{\pi}}{4\sqrt{ABC}} \quad (8)$$

Then

$$q_{max}=\frac{4Qf_r\sqrt{ABC}}{\pi\sqrt{\pi}} \quad (9)$$

The coordinate value in the semiaxis of ellipsoid is $x=a_r$, $y=b_h$, $z=c_h$. Generally, 95% heat energy is assumed to be concentrated in the half-ellipsoid, then

$$q(a_r,0,0)=q_{max}\exp(-Aa_r^2)=0.05q_{max} \quad (10)$$

Thus, the volume distribution coefficient A can be calculated as follow:

$$A=\frac{3}{a_r^2} \quad (11)$$

In the same way, other volume distribution coefficients B and C has been givn.

$$B=\frac{3}{b_h^2} \quad (12)$$

$$C=\frac{3}{c_h^2} \quad (13)$$

Therefore, the Eq. (3) can be calculated as follow:

$$q_r(x,y,z)=\frac{12Qf_r}{\pi\sqrt{\pi}\,a_rb_hc_h}\exp\left(-\frac{3x^2}{a_r^2}-\frac{3y^2}{b_h^2}-\frac{3z^2}{c_h^2}\right) \quad (14)$$

And

$$q_f(x,y,z)=\frac{12Qf_f}{\pi\sqrt{\pi}\,a_fb_hc_h}\exp\left(-\frac{3x^2}{a_f^2}-\frac{3y^2}{b_h^2}-\frac{3z^2}{c_h^2}\right) \quad (15)$$

For some little area ΔV in the left half-ellipsoid, the heat absorbed from laser can be calculated according to the endothermic formula:

$$Q=mc(T_r-T_0)=q(r)\cdot\Delta V \quad (16)$$

Therefore, the temperature T_r has been obtained as follow:

$$T_r=\frac{12Qf_r\cdot\Delta V}{mc\pi\sqrt{\pi}\,a_rb_hc_h}\exp\left(-\frac{3x^2}{a_r^2}-\frac{3y^2}{b_h^2}-\frac{3z^2}{c_h^2}\right)+T_0 \quad (17)$$

In the same way, the other temperature T_f in the right half-ellipsoid has been given by:

$$T_f=\frac{12Qf_f\cdot\Delta V}{mc\pi\sqrt{\pi}\,a_fb_hc_h}\exp\left(-\frac{3x^2}{a_f^2}-\frac{3y^2}{b_h^2}-\frac{3z^2}{c_h^2}\right)+T_0 \quad (18)$$

Where m is the mass of ΔV in the left or right half-ellipsoid molten pool; c is the specific heat of melt metal; T_0 is the original temperature ΔV.

The experimental results have indicated that the convection of molten pool is the key factor influencing the distribution of pores and elements. However, it depends on surface tension gradient which resulted from the non-uniform distribution of molten temperatures. Such surface tension gradient makes the melt metal flowing form the low tension part to the high one then molten pool convection formed.

The surface tension σ is the function of molten pool temperature and $\sigma\propto 1/T$, which presents that it descends with the increasing of temperatures. Therefore, according to the Eq.17, 18, the relations between the surface tension gradient $\mathrm{d}\sigma/\mathrm{d}x$ and molten pool temperature can be formulated as follows[13]:

$$\frac{\mathrm{d}\sigma}{\mathrm{d}x}=-c\left(1+\ln\frac{T_r}{T_0}\right)\frac{\mathrm{d}T_r}{\mathrm{d}x} \quad (19)$$

Where $\mathrm{d}\sigma/\mathrm{d}T_r$ is the surface tension temperature coefficient, $\mathrm{d}T_r/\mathrm{d}x$ is the temperature gradient of molten pool, c is the specific heat of melt metal. Simultaneously, relations between the surface tension gradient $\mathrm{d}\sigma/\mathrm{d}x$ and convection accelerated speed of molten pool has been given by[14]:

$$\frac{\mathrm{d}\sigma}{\mathrm{d}x}=\rho\Delta\alpha \quad (20)$$

Where ρ is the density of metal; Δ is the thickness of convection layers; α is the convection accelerated speed. Consequently, α can be formulated as follows:

$$\alpha=\frac{1}{\rho\Delta}\cdot\frac{\mathrm{d}\sigma}{\mathrm{d}x}=-\frac{c}{\rho\Delta}\left(1+\ln\frac{T_r}{T_0}\right)\frac{\mathrm{d}T_r}{\mathrm{d}x} \tag{21}$$

According to Eq. (21), it can be seen that the convection accelerated speed ascends with the increasing of the molten pool temperature, the temperature gradient of molten pool $\mathrm{d}T_r/\mathrm{d}x$ and the surface tension gradient $\mathrm{d}\sigma/\mathrm{d}x$ both rise. Thus the convection speed values can also be calculated by Eq.(21). For instance of pure Ni material [13], research has indicated that the convection speed is up to scopes of 1 000 mm/s as $a\approx10^2\ \mathrm{m/s^2}\sim10^5\ \mathrm{m/s^2}$ (when $\mathrm{d}\sigma/\mathrm{d}x=10^3\ \mathrm{N/m^2}$). Compared to 10 mm/s laser scanning speed, the convection speed is two orders higher than it.

Finally, longitudinal and cross section patterns of molten pool convection during laser cladding process could be shown in Fig.9[15]. The convection in the longitudinal section can be separated into two zones by the midline of molten pool, which presents that a counter-clockwise convection existing in the left zone and clockwise convection existing in the right zone (shown in Fig.9(a)). Meanwhile, there are some little convections existing in the cores of each side. The convection in the cross-section is also separated into two zones which are counter-clockwise convection existing in the left zone and clockwise convection existing in the right zone.

In a word, according to the Eq.(21) and Fig.9, it can be well illustrated the uniform distribution of elements and pores which is formed with a severe convection existing in the molten pools.

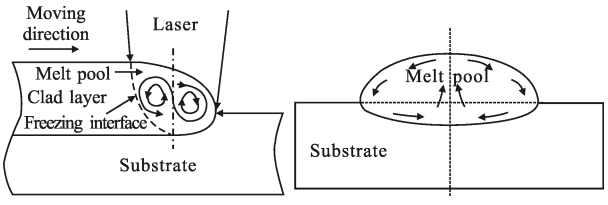

(a) Longitudinal section (b) Cross-section

Fig.9 Schematic view of molten pool convection during the process of laser cladding

3 Conclusions

(1) A severe convection exists in the molten pool during process of laser cladding which induced the uniform distribution of pores and elements in a short time.

(2) The main factors affecting pore distribution is the molten pool convection instead of the pore buoyancy. With increasing of scanning speed, pores size increases gradually and distributing location is more closed to the bottom.

(3) The convection speed is closely related to the thermal density of molten pool, the temperature distribution of molten pool and the surface tension gradient.

References:

[1] Dowden J M. The Theory of Laser Materials Processing[M]. Dordrecht: Springer Science +Business Media B V, 2008: 235-256.

[2] Li Zhuguo, Huang Jian, Wang Yaping, et al. High power diode laser cladding of Co-based alloy coating under temperature field control [J]. ***Infrared and Laser Engineering***, 2010, 39(2): 311-314. (in Chinese)
李铸国, 黄坚, 王亚平, 等. 温度场监控下高功率半导体激光熔敷钴基合金涂层 [J]. 红外与激光工程, 2010, 39(2): 311-314.

[3] Wang Weifu, Wang Maocai. Directionally deposited microstructures prepared by laser cladding +electrospark deposition[J]. ***Infrared and Laser Engineering***, 2010, 39(4): 751-755. (in Chinese)
王维夫, 王茂才. 激光+微弧火花复合定向沉积的显微组织研究[J]. 红外与激光工程, 2010, 39(4): 751-755.

[4] Athony T R, Cline H E. Heat treating and melting material with a scanning laser or electron beam [J]. ***J Appl Phys***, 1977, 48(9): 3888.

[5] Dong Wenchao, Lu Shanping, Li Dianzhong, et al. Numerical simulation of effects of the minor active-element oxygen on the marangoni convection and the weld shape [J]. ***Acta Metall Sin***, 2008, 44(2): 249-256.

[6] Xu Binshi. The theories and Technologies on Surface Engineering [M]. Beijing: National Defense Press, 1999:

429-448. (in Chinese)
徐滨士. 表面工程的理论与技术[M]. 北京: 国防工业出版社, 1999: 429-448.

[7] Salehi D, Brandt M. Melt pool temperature control using LabVIEW in Nd:YAG laser blown powder cladding process [J]. ***Int J Adv Manuf Technol***, 2006, 29(3-4): 273-278.

[8] Chen Jing, Tan Hua, Huang Weidong, et al. Evolution of molten pool shape in the process of laser rapid forming [J]. ***China J Lasers***, 2007, 34(3): 442-446.

[9] Dong Shiyun, Yan Shixing, Xu Binshi et al. Study on microstructure and mechanical property of nicufebsi alloy with laser cladding on the substrate of gray cast irons[J]. ***China J Lasers***, 2012, 39(12): 1203004-1-1203004-7. (in Chinese)
董世运, 闫世兴, 徐滨士 等. 铸铁件激光熔覆 NiCuFeBSi 合金组织及力学性能研究 [J]. 中国激光, 2012, 39(12): 1203004-1-1203004-7.

[10] Marineki B. Modern Casting[M]. Washington, D C: American Foundrymen′s Society, 1963: 99.

[11] Liu Jichang, Li Lijun, Zhang Yuanzhong. Attenuation of laser power of a focused Gaussian beam during interaction between a laser and powder in coaxial laser cladding [J]. ***J Phys D Appl Phys***, 2005, 38(10): 1546.

[12] Wu Chuansong. Thermal Process of Weld and Molten Pool Character [M]. Beijing: China Machine Press, 2007: 25-27. (in Chinese)
武传松. 焊接热过程与熔池形态 [M]. 北京: 机械工业出版社, 2007: 25-27.

[13] Zhang Yongkang. Laser Processing Technology [M]. Beijing: Chemical Industry Press, 2004: 201-202. (in Chinese)
张永康. 激光加工技术[M]. 北京: 化学工业出版社, 2004: 201-202.

[14] Zuo Tiechuan. Laser Materials Processing of High Strength Aluminum Alloys [M]. Beijing: National Defense Industry Press, 2002: 191-193. (in Chinese)
左铁钏. 高强铝合金的激光加工[M]. 北京: 国防工业出版社, 2002: 191-193.

[15] Guan Zhenzhong. Laser Processing Manual[M]. Beijing: China Metrology Publishing House, 2007: 260-264. (in Chinese)
关振中. 激光加工手册[M]. 北京: 中国计量出版社, 2007: 260-264.